Available online at www.sciencedirect.com
ScienceDirect
Acta Biomaterialia 3 (2007) 882–895
Acta BIOMATERIALIA
www.elsevier.com/locate/actabiomat

Preferred crystallographic texture of α-chitin as a microscopic and macroscopic design principle of the exoskeleton of the lobster *Homarus americanus*

D. Raabe [a,*], A. Al-Sawalmih [b], S.B. Yi [c], H. Fabritius [a]

[a] *Max-Planck-Institut für Eisenforschung, Max-Planck-Street 1, D-40237 Düsseldorf, Germany*
[b] *Max-Planck-Institute of Colloids and Interfaces, Wissenschaftspark Golm, D-14424 Potsdam, Germany*
[c] *Institut für Werkstoffkunde und Werkstofftechnik, TU-Clausthal, Agricolastr. 6, D-38678 Clausthal-Zellerfeld, Germany*

Received 5 February 2007; received in revised form 4 April 2007; accepted 16 April 2007
Available online 14 June 2007

Abstract

The crystallographic texture of the crystalline α-chitin matrix in the biological composite material forming the exoskeleton of the lobster *Homarus americanus* has been determined using synchrotron X-ray pole figure measurements and the calculation of orientation distribution functions. The study has two objectives. The first one is to elucidate crystallographic building principles via the preferred synthesis of certain orientations in crystalline organic tissue. The second one is to study whether a general global design principle exists for the exoskeleton which uses preferred textures relative to the local coordinate system throughout the lobster cuticle. The first point, hence, pursues the question of the extent to which and why α-chitin reveals preferred textures in the lobster cuticle. The second point addresses the question of why and whether such preferred textures (and the resulting anisotropy) exist everywhere in the exoskeleton. Concerning the first aspect, a strong preference of a fiber texture of the orthorhombic α-chitin is observed which is characterized by a ⟨0 2 0⟩ crystal axis normal to the exoskeleton surface for the chitin matrix. The second question is tackled by studying samples from different parts of the carapace. While the first aspect takes a microscopic perspective at the basic structure of the biological composite, the second point aims at building a bridge between an understanding of the microstructure and the macroscopic nature of a larger biological construction. We observe that the texture is everywhere in the carapace optimized in such a way that the same crystallographic axis of the chitin matrix is parallel to the normal to the local tangent plane of the carapace. Notable differences in the texture are observed between hard mineralized parts on the one hand and soft membranous parts on the other. The study shows that the complex hierarchical microstructure of the arthropod cuticle can be well described by surprisingly simple crystallographic textures.

Keywords: Anisotropy; Biological material; Composite; Plywood; Chitin

1. Motivation for the investigation of the crystallographic texture of α-chitin in different parts of the crustacean exoskeleton

Mineralized α-chitin–protein-based nano-composites such as in the exoskeleton of the lobster *Homarus americanus* occur in many modifications as cuticular materials of arthropods [1–9]. These composites, which also form the basis of the insect cuticle, have evolved over a period of 500 million years. While the structure and composition of the α-chitin–protein matrix of the arthropod exoskeleton [10–14] and the mineralization processes occurring in it [15–25] have been the objective of various studies, less attention has been paid to the investigation of the crystallographic textures of the α-chitin or of the minerals [26–35].

In this paper we therefore study systematically the orientation distributions (crystallographic texture) of the crystalline α-chitin in a biological composite material. We use the exoskeleton of the lobster *H. americanus* as a model

* Corresponding author.
E-mail address: raabe@mpie.de (D. Raabe).

1742-7061/$ - see front matter © 2007 Acta Materialia Inc. Published by Elsevier Ltd. All rights reserved.
doi:10.1016/j.actbio.2007.04.006

material. The textures are discussed in terms of pole figures and orientation distribution functions (ODFs). The pole figures were determined by standard synchrotron Bragg diffraction methods.

The study has two objectives. The first one is to elucidate whether and why preferred crystallographic orientations exist at all in such mineralized tissue. Beyond this phenomenological part of the study it is of interest to discuss whether preferred crystallographic textures in biological matter are simply a necessary by product of the biological synthesis process through which the exoskeleton material is created (synthesis theory), or whether the formation of preferred textures might follow a certain building principle with the aim of optimizing the mechanical properties of the exoskeleton (mechanical selection theory). The first approach addresses the way in which external or internal stimuli support the generation and self-assembly of such intricate though crystallographically highly organized microstructures. The second approach touches upon the question of the micromechanics that govern the relationship between the local microscopic and mesoscopic structure and the local properties of such biological nano-composites [32,36–43].

The second task of this study is to learn whether a more general construction principle exists for the whole carapace which exploits preferred crystallographic textures relative to the local coordinate system in different parts of the same exoskeleton. This point is addressed by studying samples from different sections of the carapace. When investigating biological matter from a materials science point of view, this aspect deserves particular attention since natural constructions seem to exploit the presence of structural anisotropy of their natural constituents in a more efficient and elegant way than do most man-made materials commonly used in engineering parts [32]. The connection between texture and biological design principles is at hand since a close relationship exists between the crystallographic and morphological directionalities of the microscopic ingredients of biological tissues on the one hand and the mechanical anisotropy of these materials on the other [32,36–43].

While the first aspect takes a microscopic perspective on the crystallographic nature of the material, the second point aims at building a bridge between the understanding of the microstructure and the macroscopic design of a larger biological construction when perceived as an entity.

Pursuing these questions is of interest since arthropods represent an important phylum of invertebrates that includes insects, crustaceans, and arachnids. In terms of their quantity, evolutionary age and the variety of niches they occupy, arthropods are the most successful animal group with more than one million species known. Obviously, the fabric behind the arthropod exoskeleton is a successful material which deserves analysis from the standpoint of structure and properties [5,6,8,11,15,30–45]. The decapod exoskeleton is an ideal model material for this purpose owing to the comparatively large sample sizes that can be prepared from it. An improved understanding of these aspects can help to develop corresponding man-made biomimetic nano-composites, for instance with respect to the relationship between preferred textures of artificial tissue and anisotropic mechanical properties or between textures of liquid–crystal organic fabrics and optical properties.

2. A brief introduction to the structure of the lobster exoskeleton

The American lobster *H. americanus* is a large crustacean belonging to the taxon Decapoda. Its body is divided into head (cephalon), thorax, and tail (abdomen). The thorax has five pairs of legs the first pair of which has evolved into large claws. The more slender pincher claw is used to hold the prey of the lobster while the bulkier crusher claw is used to compress it [1–3].

The physical characteristics of decapod crustaceans may vary widely between the different species. Their outer covering is referred to as exoskeleton or cuticle. Like that of most other Arthropoda, it consists of several structurally differing layers. It covers the entire body of the animal and is secreted by a single-layered epithelium. The exoskeleton provides mechanical support to the body, armor against predators, swelling protection, and enables mobility through the formation of joints and attachment sites for muscles. In order to grow, the animals must replace their old exoskeleton periodically by a new one in a process termed molting. Before the old cuticle is shed, a new, thin and not yet unmineralized cuticle is secreted by the epidermal cells. After the molt the animals expand osmotically and the new soft cuticle is completed and mineralized.

The cuticle consists of the three layers: epicuticle, exocuticle and endocuticle [1–3]. A fourth thin membranous layer is present between the three main layers and the epidermal cells during intermolt (time period between two molts). The epicuticle is the outermost layer which is thin and waxy.

The material of the exo- and the endo-cuticles is serves chiefly to resist mechanical loads [32,35,44,45]. It is a multilayered composite tissue consisting of crystalline chitin and various proteins. In crustaceans, it is usually hardened by calcium carbonate minerals (typically crystalline calcite, CC, and amorphous calcium carbonate, ACC) [6,15,20–23]. Chitin is a linear polymer of β-1,4-linked *N*-acetylglucosamine residues. This means that chitin consists of long modified glucose chains, in which a nitrogen-containing functional group replaces one of the hydroxyl groups on each glucose subunit. Chitin is a common constituent not only of the crustacean exoskeleton, but also of the arthropod cuticle in general, including insects, chelicerates, and myriapods. It also occurs in mollusk shells and fungal cell walls.

The mesoscopic structure of arthropod cuticles has been discussed in the literature [5,6,8,15,30–52]. The smallest subunits in the structural hierarchy are the chitin molecules. Their chains are arranged in an antiparallel fashion

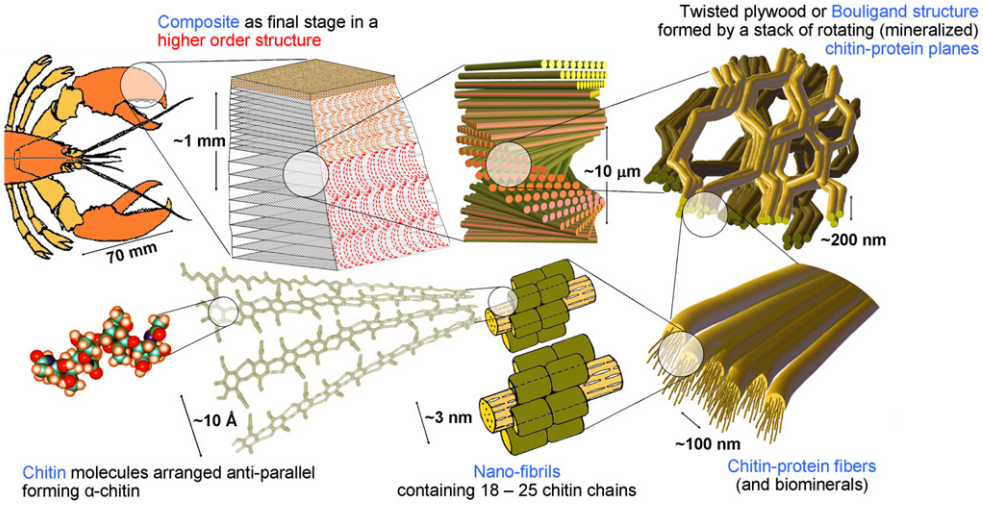

Fig. 1. Schematic presentation of the hierarchical microstructure of the cuticle of the lobster *H. americanus*.

forming α-chitin, which is the most abundant of the three crystalline chitin polymorphic forms (α-, β- and γ-chitin). Crystalline α-chitin dominates in the exoskeleton of large crustaceans; 18–25 of these chains together form nanofibrils of diameter ~2–5 nm and length ~300 nm [5]. These nanofibrils cluster to form long chitin–protein fibers with diameters between 50 and 350 nm. The fibers assemble planar honeycomb shaped arrays [31–34,46,47]. These are stacked along their normal direction forming a twisted plywood-type structure [46–48]. A stack that has been rotated from one plane to another by 180° about its normal is referred to as one Bouligand or plywood layer (Fig. 1). Characteristic for the lobster cuticle is the presence of a well-developed pore canal system with many such canals penetrating the plywood structure. The pore canals contain long soft tubes. The fibers of each chitin–protein plane are arranged around the lenticellate cavities of the pore canals, building a structure that resembles a twisted honeycomb [30–34,46–52]. In the hard parts of the lobster, the exo- and endo-cuticles are mineralized with calcium carbonate in the form of small crystallites a few nanometers in diameter. Additionally, the cuticle also contains a considerable amount of amorphous calcium carbonate. The cuticle of *H. americanus* reveals remarkable mechanical properties [32,35] which make this material an ideal candidate for materials science studies on the relationship between microstructure and properties. Details of the structure and materials science of lobster can be found in Refs. [30–35] (Fig. 1).

3. Experimental

3.1. Sample preparation

The specimens for the pole figure measurements were dissected from different parts of a large adult, non-molting American lobster (*H. americanus*). The stage of molting was determined by the presence of the membranous layer on the inner surface of the cuticle. Samples were extracted from different positions in the two chelipeds, the thorax, the abdomen and the telson, selecting both membranous and mineralized parts (Fig. 2). Immediately after killing the animal, samples were prepared by cutting rectangular pieces with a jeweler's saw. Following this, samples were washed in distilled water for 5 s, rinsed in 100% methanol for 5 s, air-dried in a fume cupboard, placed in Eppendorf caps and subsequently stored at a temperature of −70 °C. Low temperature storage before the actual measurements is required in order to suppress non-biological crystallization effects of the ACC minerals and natural decay of the polymer–protein matrix. All specimens were kept at that temperature except for the time of the actual synchrotron measurement which required ~40 min.

3.2. Structural analysis and pole figure measurement

Pole figure determination, which is also required for the calculation of ODFs [53–56], was carried out using a texture goniometer at the synchrotron radiation facility at ANKA (Angströmquelle Karlsruhe, Germany). The synchrotron measurements were conducted using the SCD (former PX) beamline operated at a wavelength of 0.8 Å, 15.5 keV and a beam size of 800 µm using as detector a CCD camera with 1024×1024 pixels (60×60 mm^2). The wide angle diffraction data were collected in transmission mode from samples with dimensions $(0.5–1.0) \times 1.0 \times 10$ mm^3 on a three-axis goniometer. One data set for each sample consisted of a series of frames taken for a sequence of phi-rotations (defined in Fig. 2) from 0° to 180° in 60 steps, each providing one Debye–Scherrer diagram. Integration was done during an exposure time of 1 min per frame. The raw diffraction data were used to calculate, via geometrical correction, normalization and beam path correction, a set of pole figures for reproducing the crystallographic textures and for the identification of different phases [30]. Fig. 2 shows experimental details and the local coordinates which were used as the

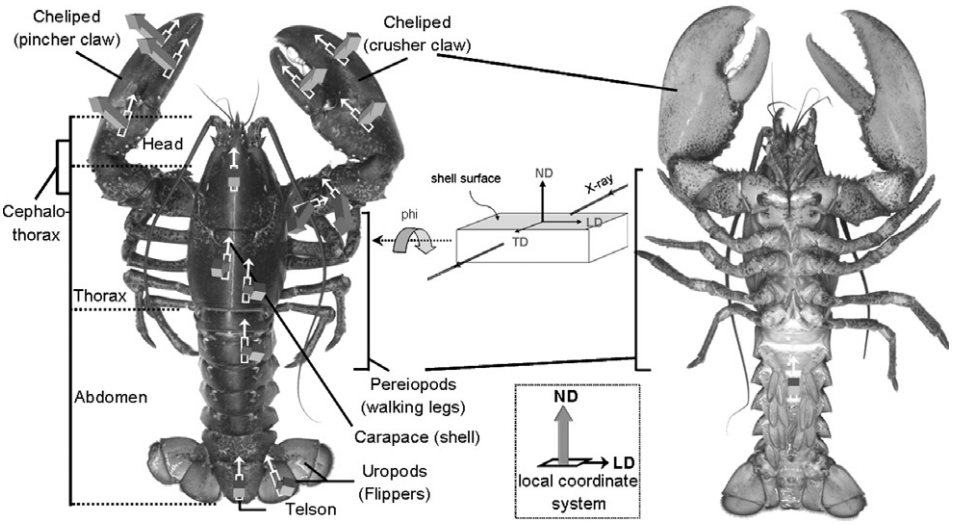

Fig. 2. Sample positions and experimental details of the coordinate system adopted during the synchrotron pole figure measurements. The figure also shows the local reference systems defined for each specimen that was selected from the cuticle for texture measurements. LD, longitudinal reference direction; ND, reference direction normal to the local sample surface; TD, transverse direction.

reference system for the various samples selected from the different parts of the exoskeleton.

Crystalline α-chitin has a density of 1.41 g cm^{-3}, a linear X-ray absorption coefficient of 3700 μm^{-1} at 14 keV (~1 Å), orthorhombic crystal structure ($a = 4.74$ Å, $b = 18.86$ Å, $c = 10.32$ Å; $\alpha = 90°$, $\beta = 90°$, $\gamma = 90°$) and space group $P2_12_12_1$ [57–65] (Fig. 3).

For structural reference matching the texture investigations outlined above, samples from locations corresponding to those of the samples used for synchrotron texture analysis were examined using high resolution scanning electron microscopy (SEM). For this purpose, the pieces from the mineralized parts of the cuticle were air-dried, cleaved in order to expose the cross-section and coated with 8 nm gold. The unmineralized membrane samples were taken from fresh specimens, rinsed in 70% ethanol, critical point dried in a Baltec CPD 030 device to avoid shrinkage and rotary shadowed with 3 nm of platinum.

3.3. Crystallographic texture analysis via the ODF

For a detailed analysis it is useful to introduce for some representative examples the corresponding ODFs [54], which provide a complete statistical description of the crystallographic texture. When using pole figures the ODFs are usually obtained by direct, Fourier-based, or component-type pole figure inversion methods [53–56]. In the current study we used the texture component method [53]. This approximates the ODF by a superposition of sets of spherical standard functions with individual coordinates, orientation density, and scatter in orientation space. Such a representation of a preferred orientation is referred to as a texture component. In contrast to the use of global symmetric Wigner functions, for instance in the Fourier-type series expansion methods [54,56], the texture component method is based on using spherical normalized localized standard functions. The superposition can be expressed by

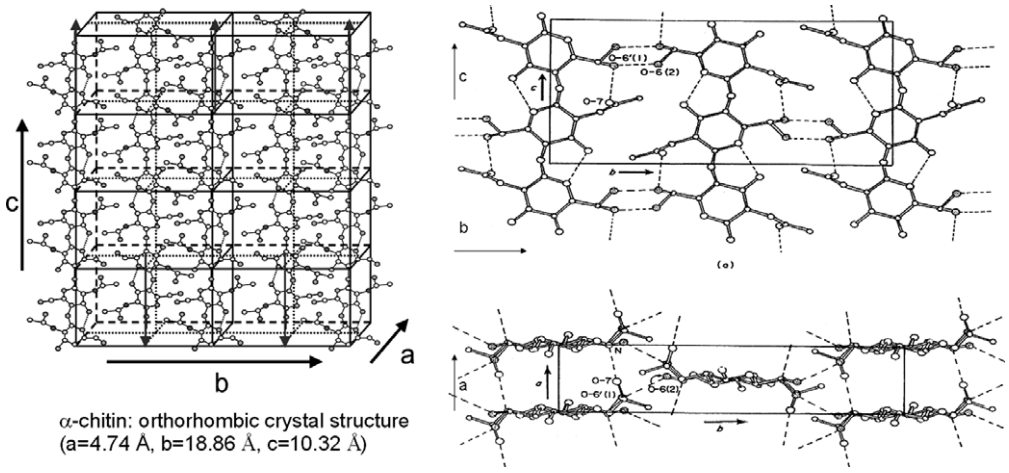

Fig. 3. Lattice structure of α-chitin according to the work of Minke and Blackwell [61]; orthorhombic symmetry ($a = 4.74$ Å, $b = 18.86$ Å, $c = 10.32$ Å), space group $P2_12_12_1$.

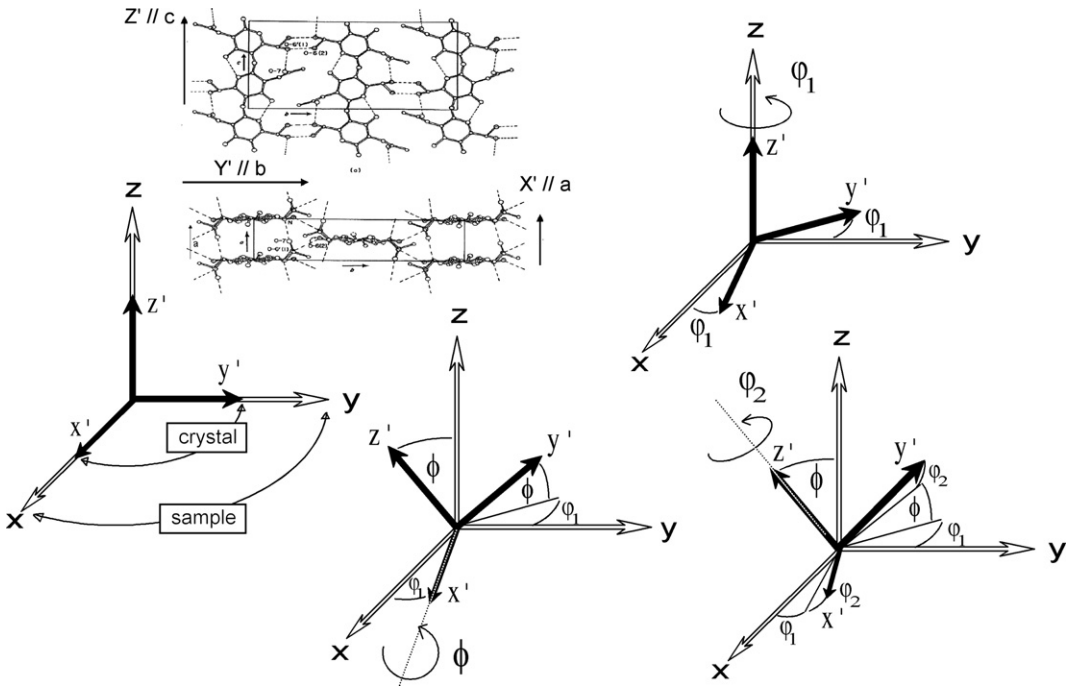

Fig. 4. Definition of Euler angles according to the Bunge rotation convention. The convention is to rotate the sample (or reference) coordinate system parallel to the crystal coordinate system in three subsequent steps. The procedure works by first rotating the sample coordinate system about the z-axis by φ_1, subsequently about the new x'-axis by ϕ and finally about the new z'-axis by φ_2. These three angles define one possible form of an orientation space in which each point represents one specific orientation.

$$f(g) = F + \sum_{c=1}^{C} I^c f^c(g) = \sum_{c=0}^{C} I^c f^c(g) \text{ where}$$
$$I^0 = F, \quad f^0(g) = 1, \tag{1}$$

where g is the orientation, $f(g)$ is the ODF, F is the volume portion of all randomly oriented crystals (random texture component), I^c is the volume portion of all crystals which belong to the texture component c. The ODF is defined by

$$f(g)\mathrm{d}g = 8\pi^2 \frac{\mathrm{d}V_g}{V} \text{ which implies } \quad f(g) \geqslant 0, \tag{2}$$

where V is the sample volume and $\mathrm{d}V_g$ the volume of all crystals with an orientation g within the orientation portion $\mathrm{d}g = \sin(\phi)\mathrm{d}\phi\mathrm{d}\varphi_1\mathrm{d}\varphi_2$.

According to the orthorhombic crystal symmetry ($a = 4.74$ Å, $b = 18.86$ Å, $c = 10.32$ Å; $\alpha = 90°$, $\beta = 90°$, $\gamma = 90°$) and the orthotropic symmetry of the local reference system (Fig. 2), the ODFs are presented in a reduced part of Euler space spanning $0° \leqslant \varphi_1 \leqslant 90°$; $0° \leqslant \phi \leqslant 90°$; $0° \leqslant \varphi_2 \leqslant 180°$. The data are presented in φ_2-sections between $\varphi_2 = 0°$ and $\varphi_2 = 175°$($\varphi_2 = 180°$ is identical to $\varphi_2 = 0°$), Fig. 4.

4. Results and discussion

Fig. 5 gives a macroscopic survey of the {0 2 0} synchrotron pole figures for the orthorhombic α-chitin which were determined for different parts of the same lobster exoskeleton according to the positions given in Fig. 2. Regular sample numbering indicates that the specimens were taken from a fully mineralized part of the cuticle (L1, L2, L3, R1, R2, R3, R4, C1, C2, C3, A1). The annex "m" indicates that the sample was extracted from a soft membranous or, respectively, telson area (Am, Rm, T1m, T2m). The "L" indicates sample positions on the pincher claw, "R" on the crusher claw, "C" on the thorax, "A" on the abdomen and "T" on the telson.

Fig. 6a and b shows the three synchrotron pole figures {0 2 0}, {0 2 1} and {0 1 3} for all specimens depicted in Fig. 5 for a more detailed analysis. The {0 2 0} pole figures are particularly important (Fig. 5) since they show the projection of the distribution of the longest crystallographic axis of the orthorhombic lattice cell ($b = 18.86$ Å) relative to the local reference system as indicated in Figs. 2–4. The projection plane is set up by the normal and the longitudinal directions as shown by the arrows in Fig. 2. This form of the {0 2 0} projection was chosen the better to elucidate the presence of the main texture components. In order to render the discussion of the occurring texture components more quantitative, Fig. 7 introduces the ODFs for two representative samples, namely, T1 (telson, example of a membranous specimen) and L2 (left claw, example of a strongly mineralized specimen). The advantage of the presentation of the pole figures (Figs. 5 and 6) is that they are usually easier to grasp, particularly in the case of strong fiber textures or single orientations. In contrast, the ODFs are on the one hand more abstract, but on the other hand allow for more quantitative texture analysis because they

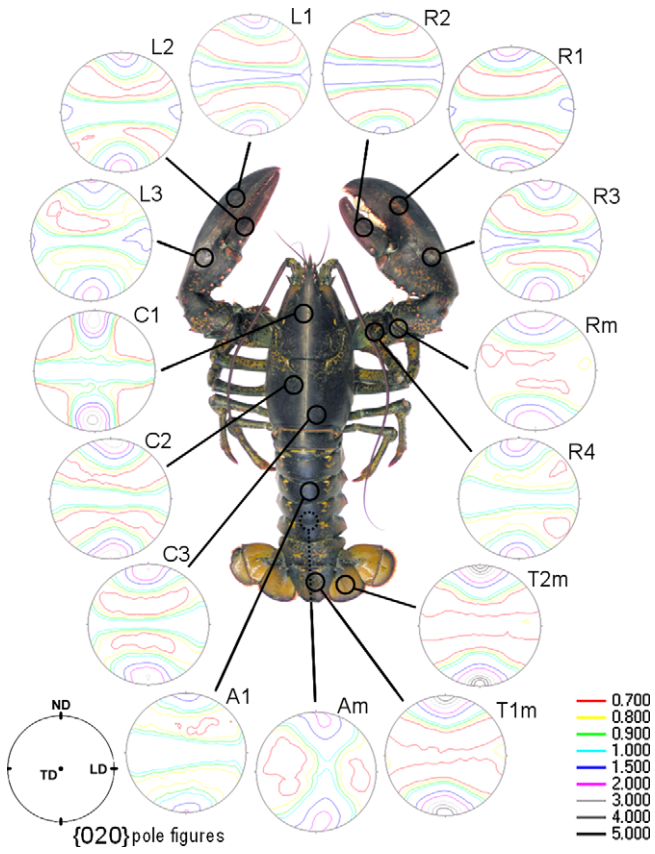

Fig. 5. Survey of the {0 2 0} synchrotron pole figures of the orthorhombic α-chitin taken from different parts of the cuticle. LD, longitudinal reference direction; ND, reference direction normal to the local surface; TD, transverse direction (see Fig. 2). Regular sample numbering indicates that the specimens were taken from a highly mineralized part of the cuticle (L1, L2, L3, R1, R2, R3, R4, C1, C2, C3, A1). The annex "m" indicates that the sample was extracted from a soft membranous or, respectively, telson area (Am, Rm, T1m, T2m). L, positions on pincher claw; R, positions on crusher claw; C, positions on thorax; A, positions on abdomen; T, positions on telson.

reproduce the true three-dimensional (3D) function of the texture as opposed to the pole figures which are projections.

The texture data presented in Figs. 4–7 show three main features. First, the most obvious property of the α-chitin in all samples is that it reveals a very pronounced crystallographic texture. This observation, which also holds for specimens taken from crabs, was already reported for single samples in Refs. [30,31,33]. Secondly, the textures of all samples, taken from different regions of the cuticle, are similar to each other. This means that the texture of α-chitin reveals similar features everywhere in the exoskeleton. Thirdly, the texture of membranous samples reveals slight differences from the textures of mineralized samples.

When referring to the first aspect, an analysis of the pole figure data in more detail shows that the crystallographic texture of the α-chitin in the lobster cuticle can be described in terms of two main texture fiber components. The first strong fiber texture component is characterized by a common ⟨0 2 0⟩ crystallographic fiber axis close to the surface normal direction. It is slightly inclined with respect to the exact normal direction by up to 10° (Figs. 5 and 6a, b). In most mineralized samples a second, weaker fiber texture can be observed. This is a fiber which is characterized by a common ⟨002⟩ crystallographic axis pointing towards the normal direction (Figs. 5 and 6a, b).

The two texture fibers can also be identified in the corresponding ODFs (Fig. 7). The relatively weak ⟨0 0 2⟩ texture fiber parallel to the surface normal runs from $\varphi_1 = 0°$ to $\varphi_1 = 90°$ at coordinates $\phi = 0°$ and $\varphi_2 = 0°$ (Fig. 7a). The more dominant ⟨020⟩ texture fiber extends from $\varphi_1 = 0°$ to $\varphi_1 = 90°$ at coordinates $\phi = 90°$ and $\varphi_2 = 0°$ (Fig. 7a and b).

Particularly, the four samples probed from the membranous (weakly mineralized) portions of the cuticle (Am, Rm) and from the telson part of the lobster (T1m, T2m) reveal a very strong fiber texture with a common normal orientation which is close to the ⟨0 2 0⟩ crystallographic axis (Figs. 5–7). The weaker ⟨0 0 2⟩ texture fiber component practically does not occur in these specimens. Fig. 6 shows that the ⟨0 0 2⟩ fiber texture component is in part inclined by up to 10° to the surface normal. Also, it can be seen that the texture does not form a completely homogeneous fiber in the membranous and telson samples, but it reveals pronounced maximum zones as visible in the {0 2 1} and {0 1 3} synchrotron pole figures (Fig. 6). Such fiber-type texture components with a preference for some main orientations are referred to as incomplete fibers. The α-chitin texture of the membranous sample referred to as Am (Figs. 2, 5 and 6), even resembles more that of a single crystal than that of an incomplete fiber. The {0 2 0} pole figure of sample Am in Fig. 6(b) shows – like the {0 2 0} pole figures of the other samples – strong {0 2 0} peaks along the normal direction, but the {0 2 1} and {0 1 3} projections clearly reveal the single crystal character of this texture. This main orientation has a strong preference for the ⟨0 2 0⟩ crystal axis (*b*-axis; see Fig. 3) which is, however, inclined by up to 10° from the surface normal reference direction (ND) and of the ⟨0 0 2⟩ crystal axis (*c*-axis, longitudinal axis of the polymer chain and of the fibrils; see Fig. 3), which is inclined by up to 10° with respect to the longitudinal reference direction (LD).

This observation suggests that a large volume fraction of the α-chitin crystals is, in the membranous samples, oriented in such a way that the long *b*-axis of the unit cell (see Fig. 3) points (with some inclination) towards the surface of the exoskeleton and the *c*-axis, which corresponds to the longitudinal axis of both the polymer chains and at the same time the chitin nanofibrils (Figs. 1, 3 and 8), points towards the longitudinal reference direction of the local coordinate system (Figs. 2 and 8).

These texture observations match our microscopic results (Figs. 9 and 10). A link between the topology of the chitin fiber orientation (topological texture) and the crystallographic fiber orientation (crystallographic texture)

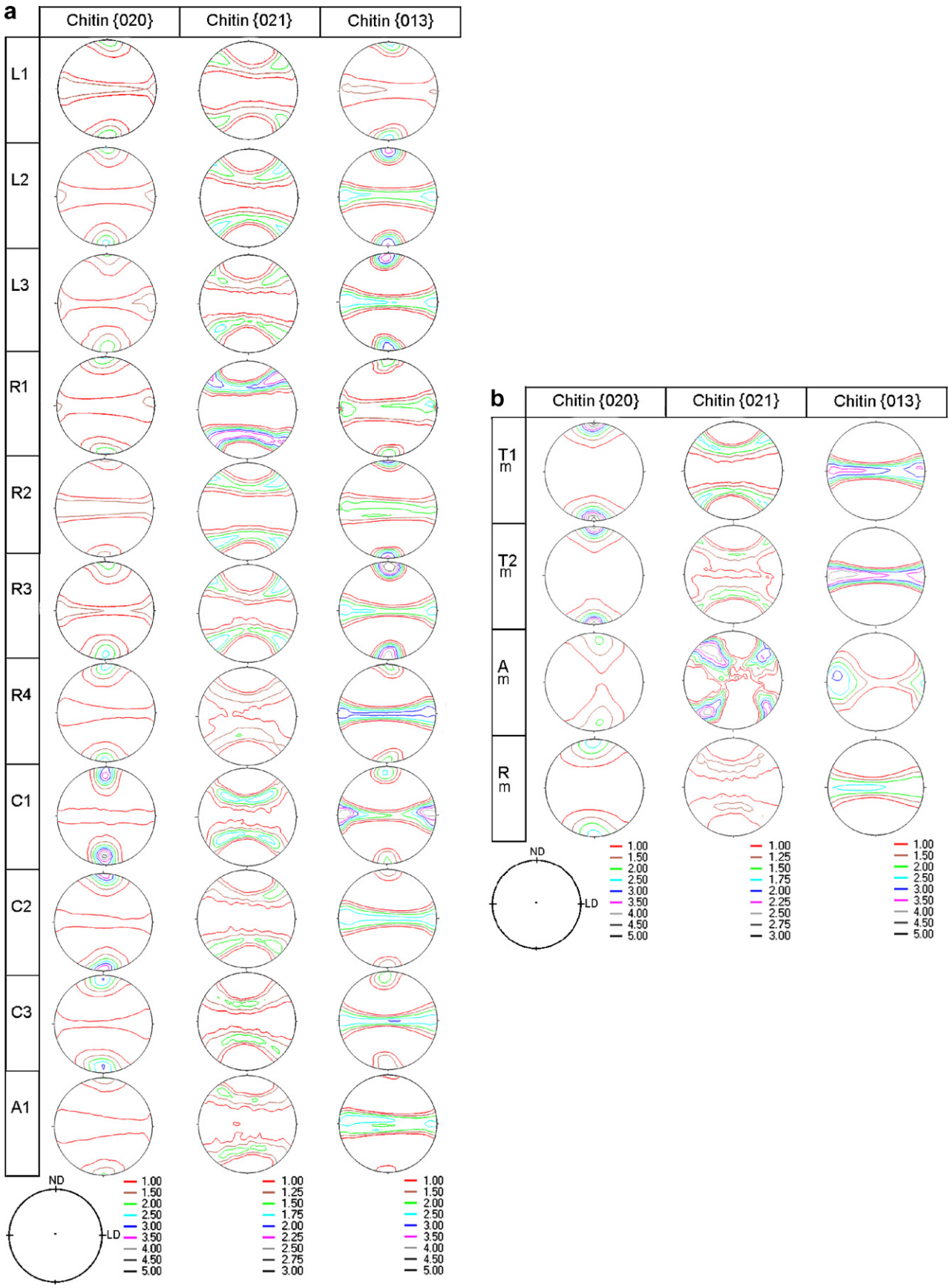

Fig. 6. Overview of the pole figures obtained by the synchrotron measurements for the orthorhombic α-chitin in different regions of the cuticle. The coordinate system and positions are indicated in Figs. 3 and 4. (a) Pole figures obtained from heavily mineralized regions of the cuticle. (b) Pole figures obtained from membranous, less mineralized regions of the cuticle.

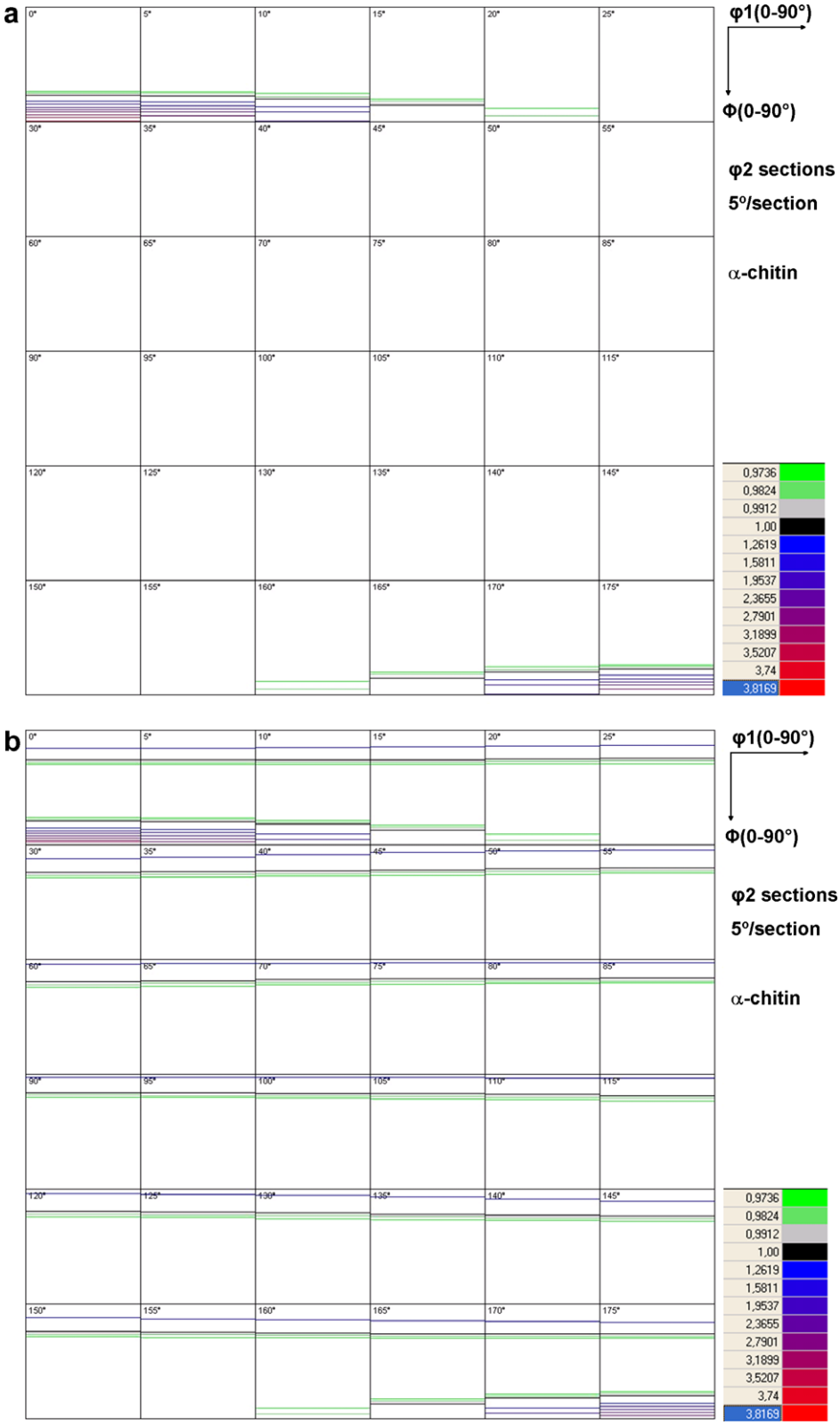

Fig. 7. Two ODFs as examples, calculated using the texture component method. (a) ODF of sample L2 obtained from a heavily mineralized region of the cuticle. (b) ODF of sample T1 obtained from a membranous, less mineralized region of the cuticle.

can be made for this composite since the *c*-axis of the orthorhombic lattice cell of the α-chitin coincides with the longitudinal axis of the chitin fibers (Figs. 9 and 10).

In contrast to the quite extreme, nearly single crystalline textures of the membranous (Am, Rm) and telson samples (T1m, T2m), the highly mineralized samples of the cuticle

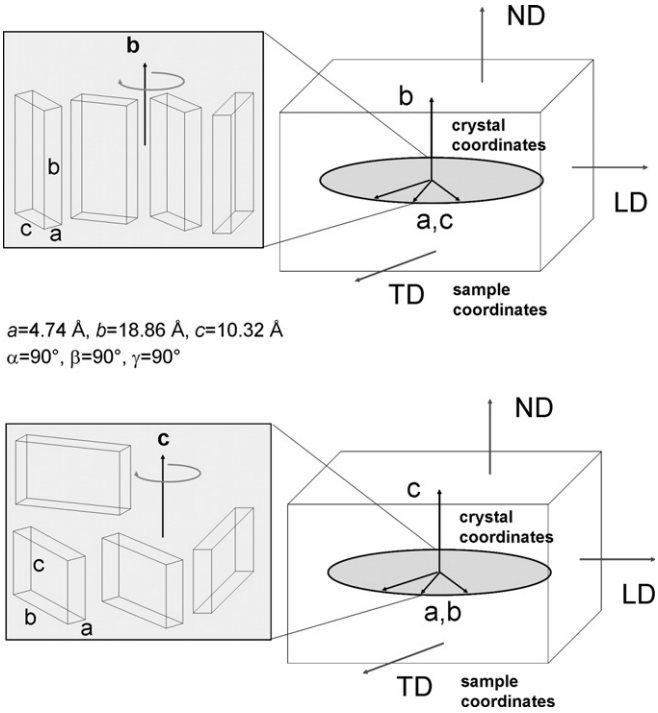

Fig. 8. Schematical presentation of the two main texture fibers. Upper row: texture fiber with the long crystallographic *b*-axis (18.86 Å) of the orthorhombic crystal lattice as fiber axis parallel to the normal of the exoskeleton (see local coordinate system in Fig. 2). Bottom row: texture fiber with the crystallographic *c*-axis (10.32 Å) of the orthorhombic crystal lattice as fiber axis parallel to the normal of the exoskeleton (see local coordinate system in Fig. 2).

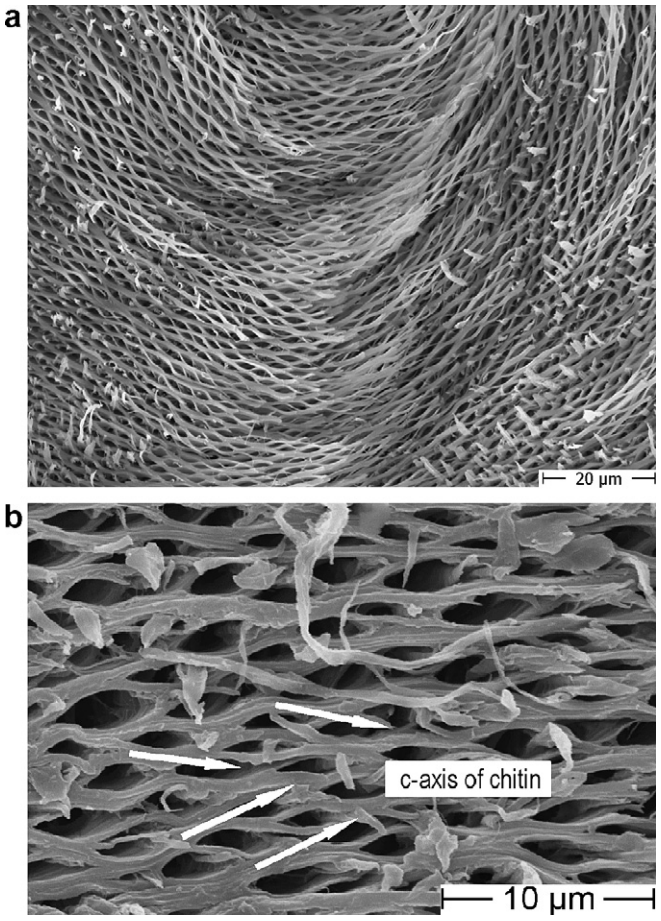

Fig. 9. Nearly flat sections of the mineralized chitin honeycomb structure (view nearly parallel to the normal direction of the cuticle). Experimental images of the helicoidal sequence (a) and inner honeycomb-like structure of the chitin–protein planes (b) within one twisted plywood layer as in-plane view. The scanning electron micrographs were taken from the endocuticle which was fractured parallel to the surface. The crystallographic [002] vectors (*c*-axis) of the chitin long crystals are indicated by arrows to show the topographic arrangement of the fibers which may explain the spread in the corresponding (002) pole figures. The long *b*-axis ([020] vectors) are normal to the images pointing to the surface of the cuticle.

(L1, L2, L3, R1, R2, R3, R4, C1, C2, C3, A1) reveal not only the same strong fiber texture parallel to the normal direction (Figs. 7–9), but they additionally show a second though less pronounced fiber perpendicular to the main one. This second fiber is characterized by a ⟨002⟩ crystal axis parallel to the normal direction. This observation suggests that the chitin–protein network of these samples reveals two fiber textures: namely, the main fiber orientation parallel to the surface and some interpenetrating fibers perpendicular to the surface. The coincidence with the presence of hose-like structures in the pore canals of the honeycomb shaped chitin–protein planes suggests that the walls of these structures are at least partially composed of chitin fibers oriented longitudinally to the long axis of the canals (Fig. 10). It is conceivable in this context that chitin is synthesized on the membranes of the cytoplasmic extensions of the pore canals. This would explain the observation that a weak ⟨002⟩ texture exists in the mineralized parts as opposed to the absence of this texture in the membranous structures which do not have pore canals. Another possibility could be that parts of the fibrous network filling the spaces of the canals consist of chitin (Fig. 10).

Some of the mineralized samples, e.g., those taken from the left claw (L2, L3), reveal a slight maximum within the ⟨002⟩//ND fiber distribution with weak maxima along the longitudinal direction (Fig. 6a). The other mineralized specimens (L1, R1, R3, R4, C1, C2, C3, A1) reveal a more continuous distribution of the {020} poles perpendicular to the ⟨002⟩//ND fiber axis.

In accord with a similar result observed in previous work [30], we assume that this slightly anisotropic distribution of the orientations along the ⟨002⟩ fiber axis can be attributed to the honeycomb structure of the woven chitin–protein network. This detail can be seen in Figs. 9 and 10 where some of the [002] vectors are indicated by arrows to show the variation in the topographic arrangement of the fibers which may explain the spread in the corresponding texture fiber. This observation matches in part the topological analysis made for the fiber alignment reported in earlier investigations [30,31,33].

The second main result in this study is that the strong texture parallel to the normal direction occurs not only in the claws as reported in earlier papers, but in all samples

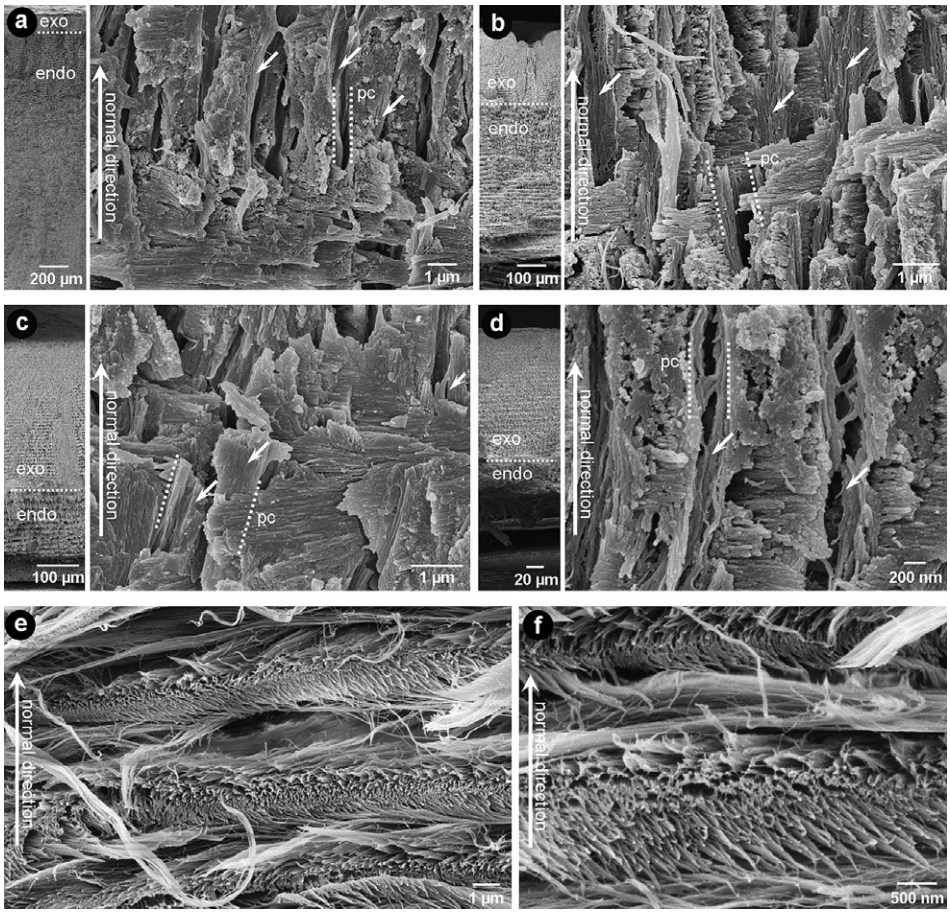

Fig. 10. Scanning electron micrographs of transversally fractured lobster cuticle from different body parts, exposing the cross-sections. (a) Cuticle from the claws; the exocuticle (exo) is thin in relation to the massive endocuticle (endo). The detail image shows fibers oriented perpendicular to the fiber planes forming the twisted plywood layers in the pore canals (pc) and lining them (arrows). (b) Cuticle from the carapace; exo- and endo-cuticle have nearly the same thickness. In the detail image, fibers oriented in the normal direction (arrows) are also present in the pore canals (pc). (c) Cuticle from the tergites; the exocuticle is about twice as thick as the endocuticle. At a higher magnification, fibers oriented in the normal direction (arrows) are again visible in the pore canals (pc). (d) Cuticle from the uropods; the exocuticle is very thick in relation to the very thin endocuticle. Fibers oriented in the normal direction (arrows) are present in the pore canals (pc) too, but their volume fraction is smaller than in the other mineralized parts of the lobster. (e) Cross-section of cuticle from the joint membranes; (f) detail image. There are no pore canals present in these unmineralized parts of the lobster; fibers oriented in directions other than in plane with the cuticle surface can not be observed.

wherever they were taken, provided that the local coordinate system serves as a reference system (Figs. 2, 5 and 6). This means that the preferred textures discussed above not only document a local microscopic construction feature of one specific portion of the exoskeleton, but also represent a building principle which seems to be common to the entire structure at a macroscopic scale.

Although the crystallographic data very clearly show the occurrence of one dominant fiber texture for all samples, it is not obvious how this finding should be interpreted. Two arguments can be put forward to explain this strong preference for a certain texture in all parts of the exoskeleton (Fig. 5). The first is that during biological evolution this crystallographic arrangement of the α-chitin matrix relative to the local coordinates turned out to be mechanically favorable, providing maximum protection against external loads. This assumption suggests the existence of a general mechanically motivated construction principle for the cuticle which is based on the crystallographic mechanical anisotropy of the α-chitin lattice (and possibly also of the other composite ingredients). Although this speculation seems to be attractive at first view, some points exist which make this hypothesis of evolution by mechanical selection difficult to confirm or reject. First, the elastic modulus tensor C_{ijkl} of the α-chitin lattice is not exactly known, i.e., any reasoning that a certain lattice direction is preferred owing to its elastic stiffness is rather speculative in the absence of generic data on the elastic tensor. Another aspect to be considered in this discussion is the fact that the strong preference of the crystallographic ⟨020⟩ texture fiber of the crystalline chitin parallel to the cuticle normal direction is likely to play an important role as an orientation template. This means that we observe an orientation relationship between the crystalline calcite and the crystalline chitin

leading to an altogether strongly textured compound. Thus, not only the anisotropy of the chitin, but also that of the co-aligned crystalline calcium carbonate have to be considered in the context of texture-guided materials design. This aspect will be presented in a subsequent paper. Although some earlier studies have published stiffness data about chitin-based cuticle, these were integral structural stiffness data of the entire nanocomposite and not of the chitin alone, i.e., these integral data must not be confused with the elastic tensor of the α-chitin lattice.

Nishino et al. [66] have published data for the elastic modulus of the crystalline regions of chitin and chitosan which they obtained by X-ray diffraction. They reported that the elastic moduli of the (dry) crystalline regions of α-chitin and chitosan in the direction parallel to the chain axis amounted to 41 GPa for α-chitin at 20 °C. Ker [67] reported a value of 20 GPa measured parallel to the chitin orientation in the tibial flexor apodeme of the locust. Yamaguchi et al. [68] have reported even smaller numbers for the modulus of chitin, namely, 8.47 GPa. However, since this value was obtained from tensile tests it is likely that it represents the net structure modulus of the entire microstructure rather than the elastic modulus of one single chitin fiber. In this context one should also mention that two authors have reported explicit values for the stiffness of the chitin lamella (and not for a homogenized tensile specimen). Xu et al. [69] have reported values for the Young's modulus for single chitin fibers of the order of 100–200 GPa. This large value is in line with a report of Vincent [5] who stated that the modulus of chitin lamellae might be as large as 130 GPa or even higher. Some considerations with regard to the bonding in the chitin lattice may help in the argumentation: the *c*-axis of the cell which is identical with the longitudinal direction of the fiber is essentially established by covalent bonds. The other two directions, *a* and *b*, are mainly connected by hydrogen bonds. The *c*-direction of the lattice should, therefore, most likely be the stiffest direction of the lattice. The experimental data of Nishino et al. [66], Ker [67], and Xu et al. [69] which were taken in the longitudinal direction of the chitin fibers, therefore suggest a lower bound value of 20 GPa [67] and an upper bound value of 100–200 GPa [69] for the stiffest direction (*c*-axis). This means that the estimate of Vincent [5] is plausible with a value of ~130 GPa. In turn, this means that the other two directions, in particular the *b*-direction which strongly prevails parallel to the normal direction, might be less stiff than the *c*-direction by up to one order of magnitude. The latter assumption is made on the basis of typical differences between covalent bonds and hydrogen bonds observed in organic crystals. These considerations seem to indicate that the observed strong ⟨0 2 0⟩ texture of the chitin is structured in such a way that not the hardest but the softest chitin direction is parallel to the surface normal.

A second point which renders the discussion of a mechanically driven selection mechanism difficult is the fact that the directionality and magnitude of the stiffness of the composite depends on different factors. These are, for instance, the amount, size, and dispersion of the calcite minerals or the density and structure of the chitin–protein matrix. This means that the crystallographic orientation of the chitin matrix does not alone determine the mechanical anisotropy of the composite [32]. Recent indentation experiments [70] have also revealed that even for samples with similar crystallographic texture, pronounced differences in the structural mechanical response can be found for different microstructures along different directions. In summary, one has to state that the idea of the prevalence of the strong ⟨0 2 0⟩ chitin texture via biological evolution through mechanically motivated selection can at this stage not be proven owing to a lack of knowledge of the overall (integral) mechanical anisotropy of the composite material.

An alternative hypothesis of why such strong and similar crystallographic textures exist in so many different areas of the same exoskeleton might be the mechanism by which the chitin filaments are synthesized. Bouligand and Giraud-Guille suggested in their work [46–52] on the twisted plywood structure of biological tissues (chitin- and collagen-based composites) that the helical organization of the chitin–protein layers might originate from a transient liquid crystal state. In a recent work, Belamie et al. [71] discussed the formation of complex hierarchical biological substructures in terms of a disordered liquid to ordered liquid phase transformation mechanism. In this approach, which goes back to the early work of Bouligand and Giraud-Guille [46–52] in this field, self-assembly is assumed to produce the observed complex ordering phenomena of biological macromolecules. The authors showed, from own work and from earlier papers which they reviewed, that the condensed state of biological macromolecules can undergo mesophase transitions when they occur as suspensions of rodlike particles. While highly dilute suspensions of fibrillar organics such as chitin (and also of collagen in compact bone [72]) are isotropic, i.e., the macromolecules assume a random orientation distribution in the fluid, an ordered nematic phase may appear beyond a critical density of the particles, often assuming a helical structure in the form of a cholesteric phase. For instance, Giraud-Guille recently showed that highly concentrated solutions of purified collagen molecules spontaneously formed ordered assemblies. These structures were then characterized by polarizing microscopy as cholesteric phases [73]. The author suggested that this particular state of matter joins both fluidity and order and could correspond to a transient state of the chitin (or collagen) secretion process, before the subsequent stiffening of these skeletal structures, bone or cuticle, via molecular cross-links and biomineralization.

Concerning this part of the discussion, it is, however, important to note that the topological arrangement of the chitin structure (topological texture) is not necessarily in all cases identical to the crystallographic texture. Such a connection is only admitted (as in the current case) if the crystallographic textures of the crystals and the

topological textures of the fibers coincide. In the present material this is the case since the *c*-axis of the chitin lattice cell is identical to the longitudinal axis of the fibers.

A third, more biological hypothesis which deserves attention when explaining the observed strong textures is the possibility of a need for a material that can be uniformly digested on its inner surface during apolysis making way for the formation of a new cuticle.

A final thought in this discussion concerns the interesting contradiction between the well-documented very complex hierarchical microstructure of the arthropod cuticle on the one hand (this paper and Refs. [1–9,14–17,27–52,71–73]) and the surprisingly simple crystallographic textures by which it can be described. This final aspect might be a new and probably helpful result when aiming at a systematic description of such complicated structures with the help of textures.

5. Conclusions

We used synchrotron wide angle diffraction to investigate the crystallographic texture of α-chitin in the exoskeleton of the lobster *H. americanus*. The main results are as follows:

- A strong ⟨020⟩//ND texture was observed in the α-chitin for all samples.
- In the membranous samples, a ⟨020⟩//ND texture fiber was the only texture component.
- Heavily mineralized samples also revealed a weak ⟨002⟩//ND fiber texture in addition to the strong ⟨020⟩//ND texture fiber.
- Samples taken from different parts of the exoskeleton revealed a similar crystallographic texture, except for the difference pointed out above between membranous and mineralized samples. This means that the α-chitin has everywhere a very similar orientation with respect to the cuticle surface. This arrangement shows that the presence of preferred chitin fiber orientations is not only a microscopic building principle, but also reflects a global characteristic of the entire exoskeleton.
- We have discussed the phenomenon of the existence of strong textures (and, consequently, anisotropy) both at microscopic and macroscopic scales, in terms of three possible mechanisms: namely, the mechanical selection theory, the synthesis theory, and the digestion theory. The first approach refers to the idea that during biological evolution the strong crystallographic arrangement of the α-chitin matrix relative to the local sample coordinates turns out to be mechanically favorable, providing maximum protection. The second approach refers to the possibility that the observed textures might be due to the liquid crystal self-assembly mechanism by which the chitin filaments are synthesized. This effect might entail the observed helical structure in the form of a cholesteric phase. The third hypothesis is that a uniform material arrangement might play a role during digestion of the inner surface during apolysis.
- It was found that the complex and hierarchical microstructure of the arthropod cuticle can be described by a surprisingly simple texture. This might be a new and helpful consideration when aiming at a systematic description of such complicated microstructures. It seems that behind the complex hierarchical structure of the chitin matrix there exists a remarkably simple crystallographic building principle.

Acknowledgements

The authors are grateful to the Deutsche Forschungsgemeinschaft (German Research Foundation) which is funding this study under the framework of the Gottfried Wilhelm Leibniz award. Kind support by colleagues at the synchrotron source at ANKA (Karlsruhe, Germany) is gratefully acknowledged.

References

[1] Vernberg FJ, Vernberg WB. The biology of crustacea. New York: Academic Press; 1983.
[2] Horst MN, Freeman JA, editors. The Crustacean Integument, Morphology and Biochemistry. Ann Arbor, MI: CRC Press; 1993.
[3] Travis DF. Structural features of mineralization from tissue to macromolecular levels of organization in the decapod Crustacea. Ann NY Acad Sci 1963;109:177–245.
[4] Hadley NF. The arthropod cuticle. Sci Am 1986;255:98–106.
[5] Vincent JFV. Arthropod cuticle: a natural composite shell system. Compos: Part A 2002;33:1311–5.
[6] Roer RD, Dillaman RM. The structure and calcification of the crustacean cuticle. Am Zool 1984;24:893–909.
[7] Neville AC. Biology of fibrous composites. Cambridge: Cambridge University Press; 1993.
[8] Dillaman RM, Hequembourg S, Gay M. Early pattern of calcification in the dorsal carapace of the blue crab, *Callinectes sapidus*. J Morphol 2005;263:356–74.
[9] Weiner S, Addadi L. Design strategies in mineralized biological materials. J Mater Chem 1997;7:689–702.
[10] Andersen SO. Biochemistry of insect cuticle. Ann Rev Entomol 1979;24:29–61.
[11] Blackwell J, Weih M-A. Structure of chitin–protein complexes: ovipositor of the ichneumon fly, *Megagrhyssa*. J Mol Biol 1980;137:49–60.
[12] Andersen SO. Exoskeletal proteins from the crab *Cancer pagurus*. Comp Biochem Phys Part A 1999;123:203–11.
[13] Shen Z, Jacobs-Lorena M. Evolution of chitin-binding proteins in invertebrates. J Mol Evol 1999;48:341–7.
[14] Hunt S, El Sherief A. A periodic structure in the pen chitin of the squid, *Loligo vulgaris*. Tissue Cell 1990;22a:191–7.
[15] Compère Ph. Fine structure and morphogenesis of the sclerite epicuticle in the Atlantic shore crab, *Carcinus maenas*. Tissue Cell 1995;27:525–38.
[16] Compère Ph, Morgan JA, Winters C, Goffinet G. X-ray microanalytical and cytochemical study of the mineralization process in the shore crab cuticle. Micron Microsc Acta 1992;23:355–6.
[17] Lowenstam HA. Minerals formed in organisms. Science 1981;211:1126.
[18] Miikkelsen A, Engelsen SB, Hansen HCB, Larsen O, Skisted LH. Calcium carbonate crystallization in the α-chitin matrix of the shell of

pink shrimp *Pandulus borealis* during frozen storage. J Cryst Growth 1987;117:125.
[19] Mann S, Webb J, Williams RJP. Biomineralization. New York: VCH Press; 1989.
[20] Lowenstam HA, Weiner S. On biomineralization. New York: Oxford University Press; 1989.
[21] Mann S. Biomineralization and biomimetic materials chemistry. J Mater Chem 1995;5:935.
[22] Manoli F, Koutsopoulos S, Dalas E. Crystallization of calcite on chitin. J Cryst Growth 1997;182:116–24.
[23] Epple M. Biomaterialien und biomineralisation (in German). Germany: Teubner; 2003.
[24] Iijima M, Moriwaki Y. Orientation of apatite and organic matrix of *Lingula unguis* shell. Calcified Tissue Int 1990;47:237.
[25] Raz S, Weiner S, Addadi L. Formation of high magnesian calcites via an amorphous precursor phase: possible biological implications. Adv Mater 2000;12:38–42.
[26] Falini G, Fermani S, Gazzano M, Ripamonti A. Oriented crystallization of vaterite inside collagenous matrices. Chem Eur J 1998;4:1048–952.
[27] Falini G, Fermani S, Ripamonti A. Oriented crystallization of octacalcium phosphate into β-chitin scaffold. J Inorg Biochem 2001;84:255–8.
[28] Belcher AM, Wu XH, Christensen RJ, Hansma PK, Stucky GD, Morse DE. Control of crystal phase switching and orientation by soluble mollusk shell proteins. Nature 1996;381:56.
[29] Weiner S, Talmon Y, Traub W. Electron diffraction of mollusc shell organic matrices and their relationship to the mineral phase. Int J Biol Macromol 1983;5:325.
[30] Raabe D, Al-Sawalmih A, Romano P, Sachs C, Brokmeier H-G, Yi S-B, et al. Structure and crystallographic texture of arthropod biocomposites. Mater Sci Forum 2005;495–497:1665–74.
[31] Raabe D, Romano P, Sachs C, Al-Sawalmih A, Brokmeier H-G, Yi S-B, et al. Discovery of a honeycomb structure in the twisted plywood patterns of fibrous biological nanocomposite tissue. J Cryst Growth 2005;283:1–7.
[32] Raabe D, Sachs C, Romano P. The crustacean exoskeleton as an example of a structurally and mechanically graded biological nanocomposite material. Acta Mater 2005;53:4281–92.
[33] Raabe D, Romano P, Sachs C, Fabritius H, Al-Sawalmih A, Yi SB, et al. Microstructure and crystallographic texture of the chitin–protein network in the biological composite material of the exoskeleton of the lobster *Homarus americanus*. Mater Sci Eng A 2006;421:143–53.
[34] Raabe D, Romano P, Al-Sawalmih A, Sachs C, Servos G, Hartwig HG. Mesostructure of the Exoskeleton of the Lobster *Homarus americanus*. Mater Res Soc Sympos Proc 2005;874, L.5.2: 155–60.
[35] Raabe D, Sachs C Mechanical properties of the lobster cuticle. Mater Res Soc Sympos Proc 2005;874, L.5.3:161–6.
[36] Gao H, Ji B, Jaeger IL, Arzt E, Fratzl P. Materials become insensitive to flaws at nanoscale: lessons from nature. Proc Nat Acad Sci USA 2003;100:5597.
[37] Ashby MF, Wegst UGK. The mechanical efficiency of natural materials. Philos Mag 2004;84:2167–81.
[38] Currey JD. The failure of exoskeletons and endoskeletons. J Morphol 1967;123:1–16.
[39] Currey JD. Biocomposites: micromechanics of biological hard tissue. Curr Opin Solid State Mater Sci 1996;l:440–5.
[40] Hepburn HR, Joffe I, Green N, Nelson KJ. Mechanical properties of a crab shell. Comp Biochem Physiol 1975;50:551–4.
[41] Melnick CA, Chen S, Mecholsky JJ. Hardness and toughness of exoskeleton material in the stone crab *Menippe mercenaria*. J Mater Res 1996;11:2903–7.
[42] Vincent JFV, Wegst UGK. Design and mechanical properties of insect cuticle. Arthropod Struct Develop 2004;33:187–99.
[43] Elices M. Structural biological materials: design and structure–property relationships. New York: Pergamon Press; 2000.
[44] Sachs C, Fabritius H, Raabe D. Experimental investigation of the elastic–plastic deformation of mineralized lobster cuticle by digital image correlation. J Struct Biol 2006;155:409–25.
[45] Sachs C, Fabritius H, Raabe D. Hardness and elastic properties of dehydrated cuticle from the lobster *Homarus americanus* obtained by nanoindentation. J Mater Res 2006;21:1987–95.
[46] Bouligand Y. Aspects ultrastructuraux de la calcification chez les crabes. 7me Congres Int Microsc Elect (Grenoble) 1970;3:105–6.
[47] Bouligand Y. Twisted fibrous arrangement in biological materials and cholesteric mesophases. Tissue Cell 1972;4:189–217.
[48] Giraud-Guille M-M. Plywood structures in nature. Curr Opin Solid State Mater Sci 1998;3:221–8.
[49] Bouligand Y. Elementary processes in the growth of thin layers in biological systems. In: Beysens D, Boccara N, Forgacs G, editors. Dynamical phenomena at interfaces, surfaces and membranes. Les Houches Series: New York: Nova Science Publ.; 1993. p. 71–83.
[50] Giraud-Guille M-M, Bouligand Y. Crystal growth in a chitin matrix: the study of calcite development in the crab cuticle, in: Karnicki ZS, et al. editors, Chitin World, Wirtschaftsverlag NW Bremerhaven, 1995. p. 136–44.
[51] Giraud-Guille MM. Chitin crystals in arthropod cuticles revealed by diffraction contrast transmission electron microscopy. J Struct Biol 1990;103:232–40.
[52] Giraud-Guille M-M. Fine structure of the chitin–protein system in the crab cuticle. Tissue Cell 1984;16:75–92.
[53] Helming K, Schwarzer R, Rauschenbach B, Geier S, Leiss B, Wenk H, et al. Z Metallkund 1994;85:545.
[54] Bunge HJ. Texture analysis in materials science. London: Butterworths; 1982.
[55] Raabe D, Lücke K. Investigation of the ADC method for direct ODF approximation by means of standard functions. Phys Status Solidi (b) 1993;180:59–65.
[56] Raabe D. Examination of the iterative series-expansion method for quantitative texture analysis. Textures Microstruct 1995;23: 115–29.
[57] Takai M, Shimizu Y, Hayashi J, Uraki Y, et al. Chitin chitosan. In: Skjak-Braek G, Anthonsen T, Sandford P, editors. Proc Int Conf. London: Elsevier Applied Science; 1989. p. 475.
[58] Takai M, Shimizu Y, Hayashi J, Tokura S, Ogawa M, Kohriyama T, et al. Structure–property relationship of α- and β-chitin. ACS Sym Series 1992;489:38–52.
[59] Saito Y, Okano T, Chanzy H, Sugiyama J. Structural Study of α-chitin from the grasping spines of the arrow worm. J Struct Biol 1995;114:218–28.
[60] Blackwell J, Minke R, Gardner KA. Proceedings of the first interernational conference on chitin and chitosan. MIT Sea Grant Report 1978;108:78–87.
[61] Minke R, Blackwell J. The structure of α-chitin. J Mol Biol 1978;120:167.
[62] Blackwell J. Structure of beta-chitin or parallel chain systems of poly-β-(1-4)-N-acetyl-D-glucosamine. Biopolymers 1969;7:281.
[63] Muzzarelli RAA. Chitin. Oxford: Pergamon Press; 1977, p. 45–51.
[64] Roberts GAF. Chitin chemistry. London: Macmillan; 1992, p. 21–35.
[65] Walton AG, Blackwell J, Carr SH. Biopolymers. New York: Academic; 1973.
[66] Nishino T, Matsui R, Nakamae K. Elastic modulus of the crystalline regions of chitin and chitosan. J Polym Sci B: Polym Phys 1999;37:1191–6.
[67] Ker RF. Some structural and mechanical properties of locust and beetle cuticle. D Phil Thesis, University of Oxford. 1977.
[68] Yamaguchi I, Itoh S, Suzuki M, Sakane M, Osaka A, Tanaka J. The chitosan prepared from crab tendon I: the characterization and the mechanical properties. Biomaterials 2003;24:2031–6.
[69] Xu W, Mulhern PJ, Blackford BL, Jericho MH, Templeton I. A new force microscopy technique for the measurement of the elastic properties of biological materials. Scanning Microsc 1994;8: 499–506.

[70] Sachs C, Fabritius H, Raabe D. in preparation.
[71] Belamie E, Mosser G, Gobeaux F, Giraud-Guille M M. Possible transient liquid crystal phase during the laying out of connective tissues: α-chitin and collagen as models. J Phys Condens Mat 2006;18:115–29.
[72] Giraud-Guille M M. Twisted plywood architecture of collagen fibrils in human compact bone osteons. Calcified Tissue Int 1988; 42:167–80.
[73] Giraud-Guille MM. Liquid crystalline order of biopolymers in cuticles and bones. Microsc Res Technol 2005:27–428.